

Analysis of plasma-controlled laser evaporation of Al target in vacuum

V. I. Mazhukin,^a V.V. Nossov,^a I. Smurov^b

^a Institute of Mathematical Modeling of RAS, Miusskaya sqr 4a,
125047, Moscow, Russia

^b I.Smurov, Ecole Nationale d'Ingénieurs de St-Etienne, 58 rue Jean Parot,
42023 St.-Etienne, France

ABSTRACT

The plasma-controlled evaporation of the Al target induced by the laser pulse with intensity of 8×10^8 W/cm² and wavelength of 1.06 μm is analysed with account for the two-dimensional effects. The self consistent model is applied, consisting of the heat transfer equation in condensed medium, the system of radiation gas dynamics in evaporated substance, and the Knudsen layer model at the two media boundary. It is established that the phase transition of the target surface is controlled by the two factors: the surface temperature that depends on the transmitted radiation intensity and the plasma pressure, governed by the expansion regime. The process comes through three characteristics stages - the sonic evaporation at the beginning, the condensation during the period of plasma formation and initial expansion and, finally, the recommence of evaporation in subsonic regime after the partial brightening of the plasma. During the subsonic evaporation stage the vapour flow and the mass removal rate is much higher near the beam boundaries than in the centre due to smaller plasma counter-pressure. The vapour plasma pattern is characterised by the dense hot zone near the surface where the deposition of laser energy occurs, and rapid decrease of density outside the zone due to three-dimensional expansion. The application of the laser beam of smaller radius at the same intensity leads to the formation of more rarefied and more transparent plasma, that allows to improve the mass removal efficiency.

Keywords: Laser-induced evaporation, Mach number, Laser plasma, Radiative gas dynamics, Stefan problem

1. INTRODUCTION

Laser-induced evaporation of metal targets lies in basis of a number of applications and remains a subject of intensive studies during more than 30 years. Such a long-term interest can be explained by the variety of physical phenomena occurred (heating, melting, evaporation of the target, plasma formation) and rapid evolution of laser sources (transition to short high power pulses, decrease of beam radius, application of the radiation of ultra-violet range) [1,2].

Surface evaporation can proceed in two qualitatively different regimes [3]. If the temperature of target surface or the pressure of surrounding medium exceeds the critical values, the supercritical regime is realised and the process can be described in terms of gas-dynamic model with the single equation of state considering the condensed phase as high density gas.

The evaporation in sub-critical regime proceeds with formation of interface boundary and nonequilibrium Knudsen layer between the two phases. The process intensity can be characterised by the Mach number, equal to gas-dynamic velocity and sound speed ratio at the external boundary of the Knudsen layer [3]. At $M = 0$ the evaporation is absent, the system is in equilibrium. The $M = 1$ condition corresponds to sonic evaporation regime with maximum degree of non-equilibrium. In this regime gas-dynamic processes in the evaporated substance do not influence on the condensed medium and can be analyzed separately. In case of sub-sonic evaporation $0 < M < 1$ evolution of the two media becomes coupled [4].

On laser treatment the sonic evaporation regime is realised if constant intensity irradiation proceeds in vacuum or in medium with low counter-pressure [5]. Under the same conditions the subsonic evaporation can also be realised for variable laser intensity and after the pulse termination [6,7]. For laser irradiation in finite pressure environment (for ex-

ample, in air) the evaporation in general is subsonic [8-12]. The sonic regime can be approached for sufficiently long and constant intensity [6,8].

Plasma ignition in vapour makes the problem significantly more complicated. The plasma absorbs incident laser radiation, the target surface shadowed from the energy source cools down and evaporation terminates. The problem was studied numerically in Refs. [13-21], characterised by a variety of approaches applied to describe the evaporation. In some cases it was assumed that evaporation proceeds in sonic regime [13] or the evaporation regime was not discussed [19, 20]. The subsonic evaporation regime was incorporated in problem statement of Refs [14,15,18,21], however no information was provided concerning evaporation regime predicted in computations. Qualitatively the plasma effect on evaporation was reduced to the screening of laser radiation.

Numerical analysis of plasma effect on the kinetics of evaporation induced by microsecond laser pulse was done in Refs [16,17] in one-dimensional approximation. It was established that after the plasma formation and termination of laser heating the evaporation with low Mach number can recommence for the short time induced by the thermal radiation of the plasma. On the other stages of the process the evaporation is suppressed by the plasma pressure and, despite the high temperature of the surface, the condensation of earlier evaporated matter is predicted.

Main objective of this paper is to analyse, with account for two-dimensional effects, the plasma-controlled evaporation induced by the laser pulse with intensity of $8 \times 10^8 \text{ W/cm}^2$ and wavelength of $1.06 \mu\text{m}$. Using the model described in section 2, the stages of surface phase transformation are identified, the plasma cloud structure is described, the effect of transition to smaller beam radius is analysed.

2. PROBLEM STATEMENT

Consider two-dimensional model consisting of heat-transfer equation in condensed phase with Stefan type boundary condition at the irradiated surface, equations of radiation gas dynamics and laser radiation transfer in vapour plasma, equations of state and absorption coefficient. For mathematical description moving cylindrical co-ordinate system is introduced with the origin fixed at the target surface in the laser beam centre, the r - axis directed along the surface and the z - axis directed along the outward normal, Fig. 1.

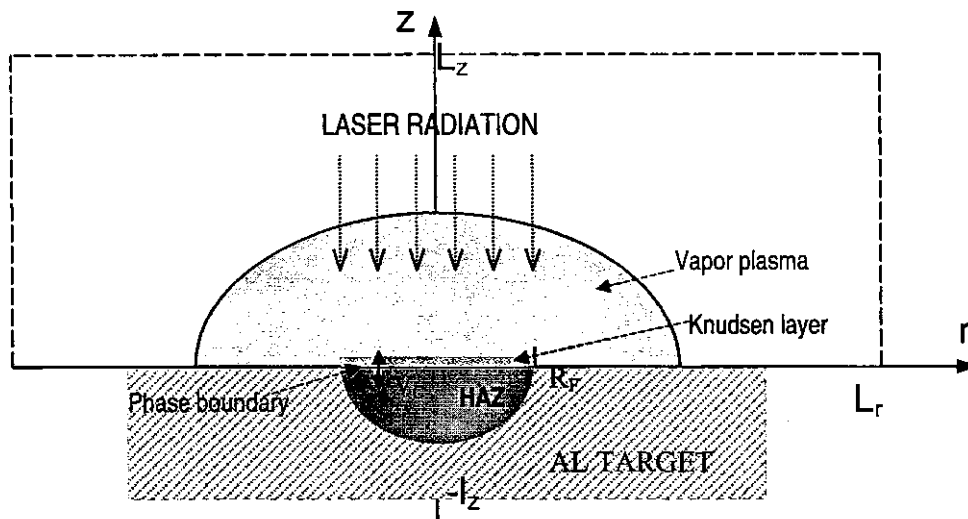


Fig. 1. Problem setup

2.1. Condensed phase

Energy transfer in the condensed phase domain $0 < r < L_r, -l_z < z < L_z$ domain is governed by heat-conduction equation [22]:

$$\frac{\partial H_c}{\partial t} + v_c \frac{\partial H_c}{\partial z} = -\text{div} \vec{W}, \quad H_c = \rho_c C_p T_c, \quad \vec{W} = -\lambda \text{grad} T_c \quad (1)$$

Here "c" index denotes the condensed phase, T_c , H_c , \vec{W} are the temperature, volumetric enthalpy and heat flux, V_c is the surface recession velocity (interface velocity), ρ_c , C_p , λ are the density, specific heat and thermal conductivity. Melting phenomenon is excluded from consideration, that has a minor influence on total energy balance because the latent heat of melting is much lower than that of evaporation. The external boundaries of the condensed domain are heat-insulated, with initial target temperature being $T_0 = 300$ K.

2.2. Gaseous phase and plasma

When the laser intensity is high enough, optical thickness of evaporated substance is sufficient to initiate an intensive absorption and avalanche ionisation. The resulting vapour plasma is partially or completely opaque for laser radiation. The work of pressure, laser energy release rate and the balance of plasma thermal radiation control its energy balance. In the vapour plasma domain $0 < (r \times z) < (L_r \times L_z)$ the system of radiation gas dynamics (RGD) equations is written [23,24]:

$$\frac{\partial \rho}{\partial t} + \text{div} \rho \vec{V} = 0 \quad (2)$$

$$\frac{\partial (\rho \vec{V})}{\partial t} + \rho (\vec{V} \cdot \text{grad}) \vec{V} = -\text{grad} P \quad (3)$$

$$\frac{\partial (\rho e)}{\partial t} + \rho \text{grad} e \vec{V} = -P \text{div} \vec{V} - \text{div} \vec{q} + \frac{\partial G}{\partial z} \quad (4)$$

$$\text{div} \vec{q}_\nu + \kappa_\nu U_\nu = \kappa_\nu U_{b\nu}, \quad \vec{q}_\nu = -\frac{1}{3\kappa_\nu} \text{grad} U_\nu, \quad U_{b\nu} = \frac{8\pi h\nu^3}{c^3 (\exp(h\nu/kT) - 1)}, \quad \vec{q} = \int \vec{q}_\nu d\nu \quad (5)$$

$$P = P(\rho, T), \quad e = e(\rho, T) \quad \kappa_\nu = \kappa_\nu(\rho, T, \nu) \quad (6)$$

where $\vec{V} = (u, v)$ is the gas-dynamic velocity, ρ , P , e are the density, pressure and volumetric internal energy respectively, $\vec{q} = (q_r, q_z)$ is the radiative heat flux, κ_ν is the absorption coefficient of plasma radiation, U_ν , $U_{b\nu}$ are volumetric density of radiation and blackbody radiation, "v" index denotes frequency dependent quantities. Eqn. (5) describes radiation transfer in diffusion approximation [25]. The equation system (2 – 6) is supplemented by the boundary conditions, considered in Ref. [24]. The equations of state and absorption coefficient (6) are calculated by the technique of Ref. [26], which is based on the Hartree – Fock – Slater model.

Laser radiation transfer equation along the z-axis accounts for incident G and reflected G^- components and is written within the laser beam domain $0 < r < r_f$, r_f is the beam radius:

$$\frac{\partial G^-}{\partial z} - \kappa G^- = 0, \quad \frac{\partial G^+}{\partial z} + \kappa G^+ = 0, \quad G = G^- - G^+, \quad 0 < z < L_z \quad (7)$$

$$z = L_z : G^- \equiv G_0 \times G(r), \quad z = L_z : G^+ = (1 - A(T))G^-$$

where $A(T)$ denotes surface absorptivity, $G(r)$ specify the type of spatial intensity distribution of the laser beam: $G(r) \equiv 1$ for the so called "top-hat" pulse or $G(r) \equiv \exp(-(r/r_f)^2)$ for Gaussian pulse shape. The absorption coefficient of laser radiation κ for the considered wavelength of infrared range $1.06\mu\text{m}$ is determined by Inverse Bremsstrahlung mechanism [25], and is calculated in assumption of equilibrium charge composition.

2.3. Interface boundary conditions

Intensive evaporation of the target starts when surface temperature exceeds some value T^* determined by background pressure. The principal feature of evaporation problem is presence of non-equilibrium domain adjacent to the surface Knudsen layer, in which the state of vapour can not be described by continuous medium equations.

In general, vapour flow leaving the surface depends on the state of already evaporated substance above the surface, which is governed by gas-dynamic equations. The boundary conditions at the surface should link six quantities: the

velocity V_c , the surface temperature T_c and pressure P_c , the vapour temperature, density and gas-dynamic velocity at the external boundary of Knudsen layer. For this purpose conservation of energy, mass and momentum is used:

$$\lambda_c \frac{\partial T_c}{\partial z} = AG^- + L_v \rho_c V_c, \quad \rho_c V_c = \rho(V_c - v), \quad \rho_c V_c^2 + P_c = \rho(V_c - v)^2 + P, \quad (8)$$

as well as two additional relations, dependent on the applied approximation of Knudsen layer [27,28]:

$$\frac{T}{T_c} = \frac{2\gamma M^2 (m^2 + 1/2)^2}{(1 + \gamma M^2)^2 m^2 t^2}, \quad \frac{\rho}{\rho_{sat}} = \frac{tm^2 (1 + \gamma M^2) (\gamma M^2 (m^2 + 1/2))^{-1}}{\exp(-m^2) + \pi^{1/2} m (1 + \text{erf}(m))} \quad (9)$$

$$M = v/\sqrt{\gamma RT}, \quad \rho_{sat} = P_{sat}/(RT_c), \quad P_{sat} = P_b \exp\left(\frac{L_v}{RT_c} \left(1 - \frac{T_b}{T_c}\right)\right), \quad R = \frac{R_0}{A} \quad (10)$$

$$f(m) = F(M)(m^2 + 1/2)^2 - m^2(m^2 + \alpha + 3/2) = 0,$$

$$F(M) = 1 + \frac{3\gamma M^2 - 1}{\gamma M^2 + 1}, \quad \alpha = 2t^2 - 2^{-1} \pi^{1/2} mt - 1, \quad t = \frac{2m}{\pi^{1/2}} + \frac{1 + \text{erf}(m)}{\exp(-m^2) + \pi^{1/2} m (1 + \text{erf}(m))},$$

Here M is the Mach number, ρ_{sat}, P_{sat} are the saturated vapour density and pressure corresponding to surface temperature T_c , L_v is the latent heat of evaporation, R, R_0, A are the gas constant, universal gas constant and atomic mass respectively, γ is the adiabatic constant equal to 5/3 for monatomic vapour, P_b, T_b are the pressure and equilibrium boiling temperature at the normal conditions.

The last undefined quantity (Mach number in our case) is determined from the solution of gas-dynamic equations. While M is found, the quantities m, t, α necessary to evaluate the relations (9) are found by solving non-linear Eqn. (10). At $M = 0$ the evaporation (convective) is absent, the total vapour flow across the boundary is equal to zero, the temperature is continuous and the vapour above the surface is in saturated state. At $M > 0$ temperature, density and pressure of vapour are discontinuous, with maximum deviation reached at $M = 1$, sonic evaporation: $T = 0.633T_c, \rho = 0.326\rho_{sat}, P = 0.203P_{sat}$. The flow of evaporated substance in this case also reaches maximum equal to 0.825 of Herz-Knudsen flow $j_{HK} = \rho_{sat} \sqrt{RT_c/2\pi}$. As it is shown in Refs. [27, 29] supersonic regime of evaporation $M > 1$ is impossible.

If $P_{sat} < P$ relation is fulfilled on the Knudsen layer ($M < 0$), then the evaporation turns into condensation. According to the results of numerical and analytical studies [21-23], only one condition is imposed on the three quantities $T/T_c, M$ and ρ/ρ_{sat} (or P/P_{sat}) in the case of subsonic condensation, for example $\rho/\rho_{sat} = F_1(T/T_c, M), P/P_{sat} = F_2(T/T_c, M)$, while the values of another two parameters T/T_c and M are controlled by the state of gas dynamic flow. At present, the analytic expressions for F_1, F_2 functions are derived only for some limiting cases, and in general they are determined numerically from Boltzmann equation and tabulated. The results of Ref. [31] are used in our model for $P/P_{sat} = F_2(T/T_c, M)$ relation. The F_2 has only weak dependence on temperature and is approximated as $P/P_{sat} \approx F^*(M) \approx 0.95 \exp(2.42M)$. In opposite to evaporation, condensation can proceed in supersonic regime.

2.4. Numerical algorithm

The differential problem is solved (1)–(10) by finite – difference (FD) technique. The computational grid along the r -axis in the $0 < r < L_r = 5$ cm domain consists of 50 – 100 nodes and is made more dense in laser action zone $0 < r < r_f$. The non-uniform grid along the z -axis is constructed separately in condensed ($L_z = 0.01$ cm, 40 nodes) and gaseous ($L_z = 10$ cm, 100–200 nodes) domains. The smallest grid steps are at the target surface and are equal 2×10^{-6} cm and 10^{-5} cm for condensed and gaseous phase, respectively. The non-linear heat transfer equation with convective term is approximated by implicit FD equation using five-point stencil [33]. The equation was solved by alternative direction method. The FD approximation and computational algorithms applied for RGD part of the model was described in details in Ref. [34]. The algorithm for the whole problem consists of the following three blocks: 1) The solution of RGD equations; 2) The evaluation of boundary conditions; 3) The solution of heat conduction equation that are iteratively executed on every time step [19].

3. RESULTS AND DISCUSSION

3.1. Processes in the beam centre

Consider processes on Al target surface irradiated by the laser pulse with constant intensity of $8 \times 10^8 \text{ W/cm}^2$, "top-hat" spatial profile, with wavelength $\lambda = 1.06 \mu\text{m}$, beam radius $r_f = 0.025 \text{ cm}$ and pulse duration of 150ns. Values of Al parameters used in computations are presented in Table 1.

Table 1. Parameters of aluminium

Variable	Value	Variable	Temperature dependence		
			$T_0 = 300\text{K}$	$T_m = 933\text{K}$	$T_{cr} = 8000\text{K}$
T_b	2720K	λ	2.37	0.75	0.16
P_b	1Bar	ρ	2.7	2.33	0.64
L_v	$1.1 \times 10^4 \text{ J/g}$	C_p	0.95	1.2	1.2
A_m	27	A	0.1	0.1	0.3

The intensity of laser radiation reaching the target is the principal parameter governing the processes on the surface. Depicted in Fig. 2 are the time development of absorbed intensity in the beam centre $G_s = AG(r = 0, z = 0)$, as well as vapour plasma transmission coefficient along the beam axis $Tr = G(r = 0, z = 0) / G_0$. At the beginning the evaporated substance above the surface is transparent and all the laser radiation reaches the surface $Tr = 100\%$, $G_s = AG_0 \approx 2.5 \times 10^8 \text{ W/cm}^2$. The system behaviour changes qualitatively when plasma is formed in the vapour. The plasma effectively absorbs the laser radiation due to high electron concentration and its action on the surface terminates, Fig. 2: $Tr \approx 0$. Later on as the plasma expands, it becomes partially transparent and starting at $t \approx 120 \text{ ns}$ the transmission coefficient remains at approximately constant level $Tr \approx 10\%$, $G_s = 2.5 \times 10^7 \text{ W/cm}^2$.

Let's return now to the main subject of our analysis – the phase transformation of the surface. The process will be characterised by the following time dependent quantities taken at the beam centre $r = 0$: surface temperature T_c , Mach number M , Fig. 3, saturated vapour pressure P_{sat} and vapour plasma pressure P_p , Fig. 4. As indicated in Fig. 3, three specific stages of the process are separated. Intensive laser energy deposition in near-surface layer courses its fast heating and in a short time the vapour flow reaches the sound velocity ($M = 1$), therefore in further consideration the stage I will be referred to as sonic evaporation. However, both the surface temperature and, as a consequence, the vapour flow velocity continue to increase. Steady-state evaporation regime is reached over $\approx 5 \text{ ns}$ at a surface temperature slightly below the critical temperature of Al ($\approx 8000\text{K}$), characterised by the equality of laser energy input G_s and the energy losses due to evaporation and conductive heat flux toward the bulk $\lambda \text{ grad}(T_c)$. As seen in Fig. 4, the condition $P_{sat} > P_p$ is fulfilled during the stage I: saturated vapour pressure is approximately 5 times higher than the plasma pressure.

After the plasma formation the energy input to the target surface terminates, its temperature and saturated vapour pressure rapidly diminishes, at $t = 20 \text{ ns}$ the $P_{sat} < P_p$ condition realises and evaporation turns to condensation, Fig. 3 and 4, Stage II, $M < 0$. Majority of time the condensation proceeds in subsonic regime. The Mach number sharply decreases and reaches the -1 value only at $t \approx 80 \text{ ns}$, when disturbance from the region of initial plasma ignition reaches the surface, Fig. 4, peak of the P_p curve.

High pressure of the plasma results in its rapid expansion. As new substance inflows from the surface to plasma is absent, the expansion leads to the partial restoration of transparency and the onset of subsonic evaporation stage, Fig. 3, 4, stage III, with very low Mach number lying near the boundary of connective evaporation $M \approx 0.03$ [4]. The comparison of evaporation on the stage I and III gives insight into the relation of temperature and gas-dynamic factors – temperature and saturated vapour pressure on the stage III are only slightly lower than that of stage I, Fig. 3, 4 however the flow is decelerated by strong plasma counter-pressure. It worth to mention that due to small Mach number the vapour density on stage III is just as high saturated vapour density $\rho(M = 0.03) \approx 0.95\rho_s$, and exceeds the vapour density on stage I $\rho(M = 1) = 0.32\rho_s$.

The effect of plasma thermal radiation is illustrated by the radiation flux reaching the surface in the beam centre $q_s = q_z(r = 0, z = 0)$, Fig. 2. On the stage II the plasma radiation is as high as $6 \times 10^6 \text{ W/cm}^2$ and it keeps the surface at relatively high temperature. On the stage III the plasma radiation flux is $\approx 10^6$ and is more than one order of magnitude weaker than the laser intensity.

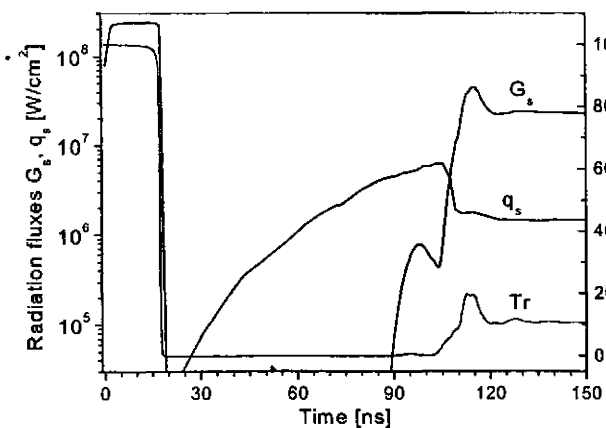


Fig. 2. Transmitted laser intensity G_s , transmission coefficient Tr and thermal radiation flux q_s vs time at $r = 0, z = 0$

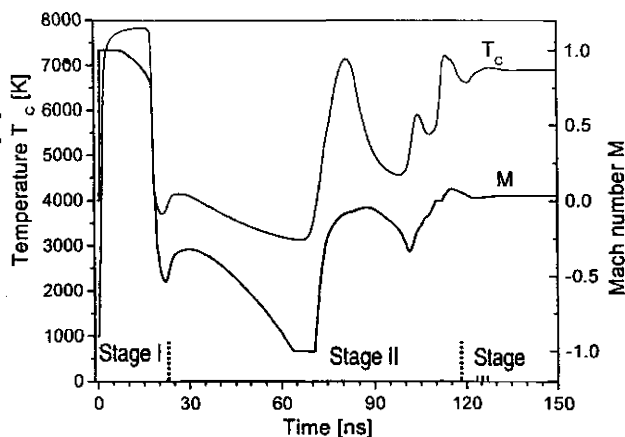


Fig. 3. Target surface temperature and Mach number vs time at $r = 0, z = 0$

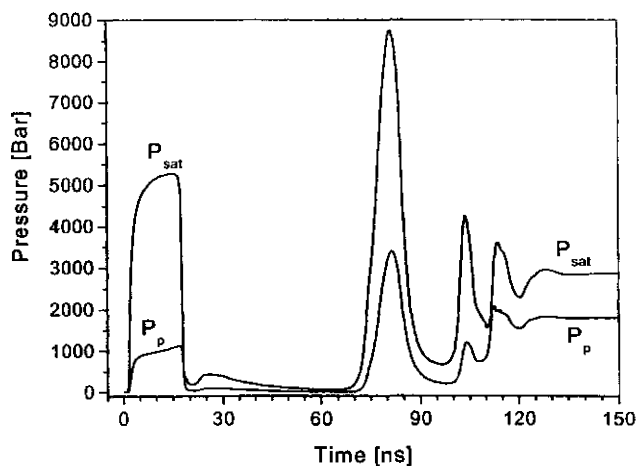


Fig. 4. Saturated vapor pressure P_{sat} and plasma temperature P_p vs time at the focal spot centre

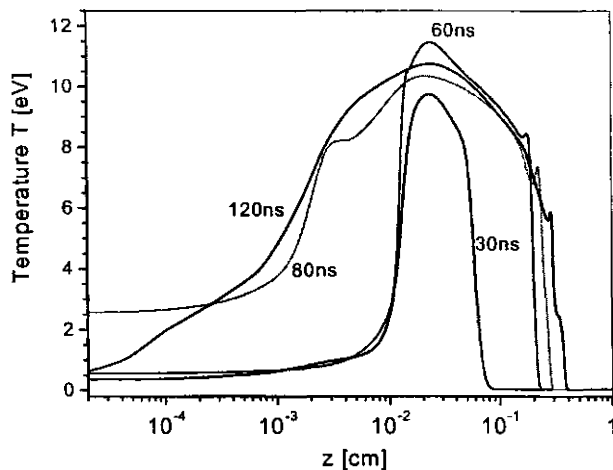


Fig. 5. Plasma temperature profiles at the beam axis

3.2. Plasma pattern structure

Consider some features of plasma pattern evolution that essentially influence the surface phase transformation. Depicted in Fig. 5 are plasma temperature profiles along the $r = 0$ axis taken at the instant of time indicated near the curve. Initially plasma is formed at the forefront of the vapour cloud at the distance of $\approx 10^{-2}$ cm from the surface, Fig. 5, 30ns. At the later points in time the plasma expands rapidly in two directions – toward the laser source and the surface. At $t = 80$ ns the ionisation front reaches the surface, and this event manifests itself as a peak of temperature and pressure in Figs. 2 and 4. Starting at 120ns the temperature profiles of steady shape slowly propagate in positive direction.

Contour plots of 2D temperature distribution taken at $t = 30$ ns and $t = 120$ ns are presented in Fig. 6. The figure 6a corresponds to the curve "30ns" in Fig. 5 and demonstrates additionally that radial expansion only begins at this instant. The instant of 120ns, Fig. 6b corresponds to steady expansion regime and is characterised by axial expansion velocity being two times as high as radial velocity. The plasma has hot core near the surface where laser energy release takes place and local temperature maximum at the forefront.

Distribution of plasma density at $t = 120\text{ns}$ is depicted in Fig.7. The curve "30ns" in Fig. 7a shows that at this instant of time the vapour/plasma density near the surface is approximately constant. Further on the density in this region decreases due to condensation, Fig 7a, 80ns. The dependency at 120ns corresponds to steady distribution. At a distance of $z \ll r_f$ from the surface the density descends linearly as the expansion is quasi-one dimensional in this domain. Outside the domain the density drops much faster $\rho \sim 1/z^3$ due to intensive lateral expansion. Therefore, despite the high temperature of the plasma cloud its major part remains transparent for the laser radiation. Shown in Fig 7b is the contour plot of the density at $t = 120\text{ns}$. It readily illustrates that major part of the plasma cloud is strongly rarefied. For example the density at a distance of 0.1 cm from the beam centre does not exceed 10^{-5} g/cm^3 .

Distributions of the degree of ionisation and electron concentration in the plasma at $t = 120\text{ns}$ calculated by Saha equations [25] are presented in Fig 8. The major part of the plasma cloud consists of single and double charged ions, Fig. 8a. The maximum degree of ionisation is as high as 3 and is reached in the region along the beam axis and at the forefront. Despite this, significant concentration of electrons is observed only in the very center of the cloud, Fig. 8b and it can be seen that the distribution is controlled primarily by the plasma density (compare with Fig 7b). It is important to note that for the rarified plasma the time needed to reach the equilibrium distribution is long enough, and the Saha formula give essentially overestimated values of the electron concentration.

The location of laser energy deposition zone is an important characteristic of the plasma pattern, Fig. 9, $G(z, r = 0)$. At $t = 30\text{ns}$ energy release takes place in the narrow region around $z \approx 10^{-2} \text{ cm}$. Further on, the absorption zone becomes wider, reaches the surface and the energy release rate $\partial G/\partial z$ diminishes.

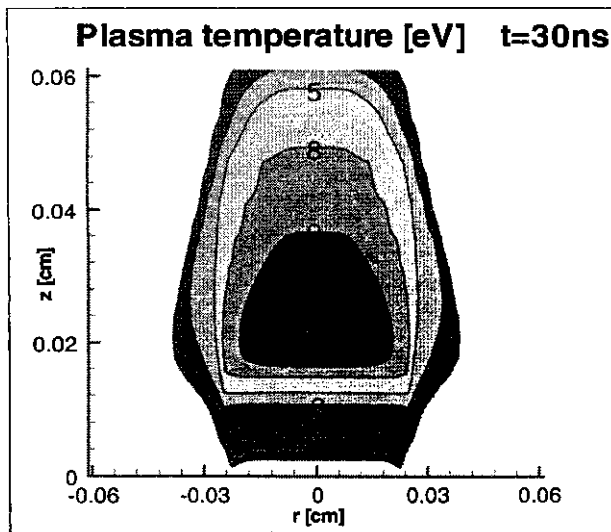
3.3. Processes on the surface

Analysis of phase transition in subsection 3.1 relates is quasi-one dimensional as it deals with only one point in the beam centre. Consider further dependency of the processes on radial co-ordinate. Target temperature profiles $T_c(r, z = 0)$ taken at several instants of time are presented in Fig. 10. At $t = 10 \text{ ns}$ the plasma in vapour has not yet formed and the temperature across the irradiation zone $|r| < r_f$ is constant, Fig. 3, stage I. The profile at $t = 30\text{ns}$ already corresponds to plasma-controlled period. The plasma completely shadows the surface and its temperature decreases to 3000–3500K. The profiles at later points in time correspond to condensation stage and demonstrate that the recommence of evaporation occurs near the beam edges at first and later with time shift of 30–40ns in the central part. This fact indicates that the brightening of the plasma is the result of not only axial plasma expansion but expansion in lateral direction as well. The latter effect manifests itself earlier at greater distance from the beam centre. At $t = 120\text{ns}$ the steady temperature distribution is established, characterised by the slow decrease from the beam edge (7200K) toward the center (6900K).

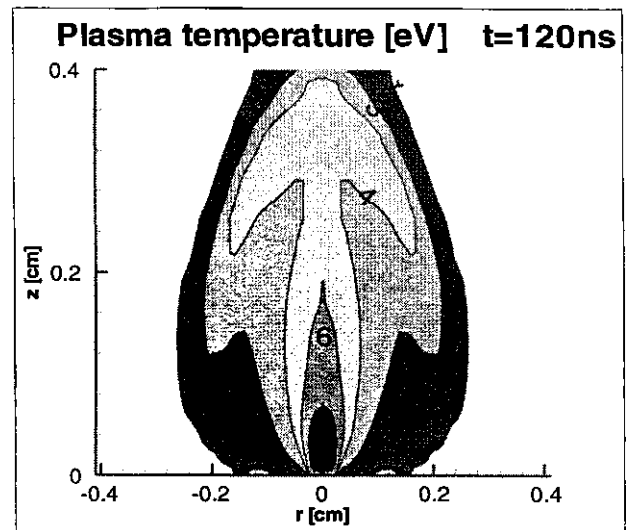
The radial expansion reduces the counter-pressure of the plasma near the boundaries of evaporation zone, so hypothetically the process should be more intensive there. The assumption is confirmed by the results in Fig. 11 showing the time development of Mach number at the surface for three specific radial points: $r = 0$, $r = r_f/2$ and $r = r_f$. The processes in the former two points goes on identically, but at the beam boundary the evaporation recommences earlier and proceeds more intensively.

Radial distributions of vapour flow (mass loss rate) from the surface $j = V_c \rho_c = u_s M \rho_v$ at two instants of time corresponding to sonic and subsonic evaporation stages are shown in Fig.12. At $t = 10 \text{ ns}$, in accordance with the above presented results the flow is constant in all the points of the irradiation domain and is $j \approx 1.1 \times 10^4 \text{ g/cm}^2\text{s}$. On the stage III, $t = 120 \text{ ns}$, the flow is much weaker. The most essential reduction is in the beam center $j = 8 \times 10^2 \text{ g/cm}^2\text{s}$ while near the beam boundary the flow is several times more intensive. The additional dotted curve illustrates the computational grid effect on the results: if the number of nodes along the r axis is less by a factor of 2 the visible change of flow ($\approx 20\%$) appears only at one point $r = r_f$.

Depicted in Fig. 13 is the amount of material removed versus radius dependencies derived by integration of surface recession velocity V_c . The curve taken at $t = 20 \text{ ns}$ shows that just before the plasma ignition the removed layer has constant thickness of approximately 2 microns. At the later instant $t = 80\text{ns}$ the thickness partially decreases due to the condensation of previously evaporated substance. Well seen hollows near the beam edges at $t = 80\text{ns}$ and especially at 150ns mean that this part of evaporation zone gives significant contribution to the total amount of removed material.

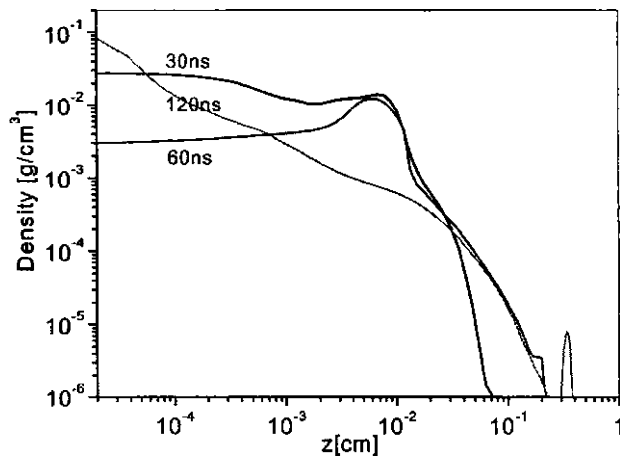


a)

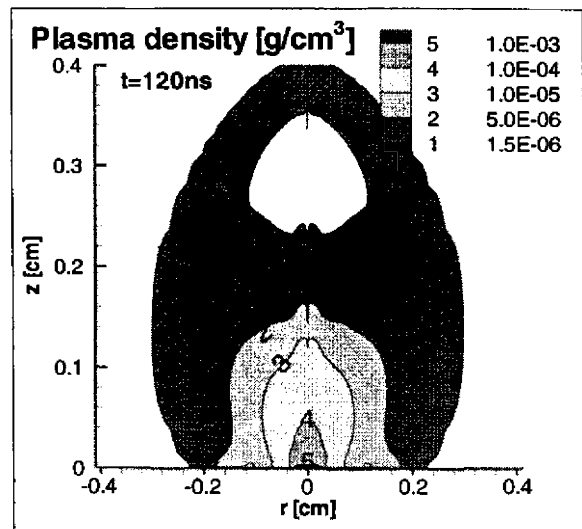


b)

Fig. 6 Contour plot of the plasma temperature at $t = 30\text{ns}$: a) and $t = 120\text{ns}$: b)



a)



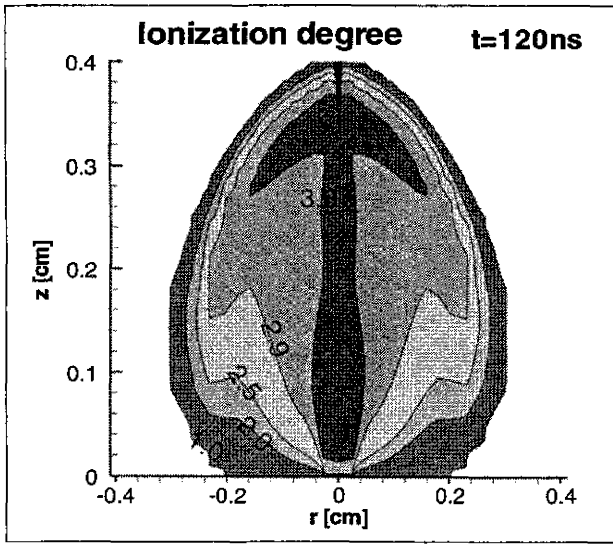
b)

Fig. 7. Plasma density profiles at the beam axis: a) and contour plot at $t = 120\text{ns}$: b)

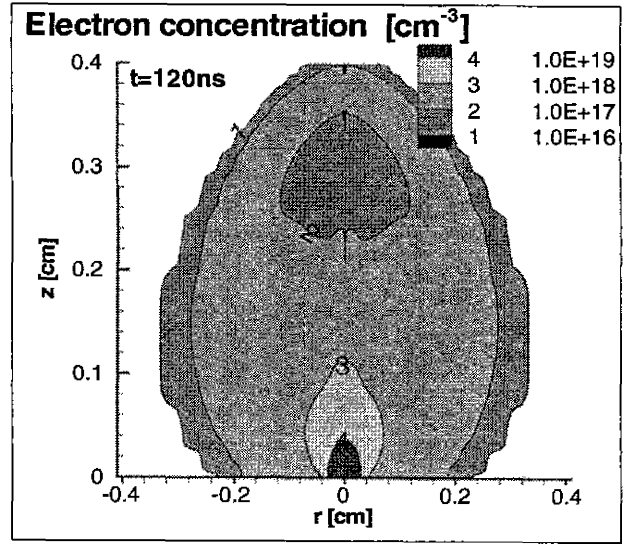
3.4. Influence of the beam radius

Two-dimensional effects in plasma-controlled evaporation should manifest itself more apparently for smaller radius of the laser beam. Analyse this phenomenon and compare the above presented results predicted for the radius of $250\ \mu\text{m}$ with the results at smaller radii $r_f = 100\ \mu\text{m}$ and $r_f = 25\ \mu\text{m}$. Time development of the processes can be compared by means of transmission coefficient plots, Fig. 14. The instants of plasma ignition coincides for all the three cases. The duration of the condensation stage shortens as the radius decreases due to smaller total amount of the matter evaporated during the stage I and more pronounced 3D expansion of the plasma. The part of radiation reaching the surface after the brightening of the plasma increases from 10% to 18% .

Temperature and density profiles taken at the beam axis at $t = 120\text{ns}$, Fig. 15, correspond to the steady state of plasma in Stage III. For smaller beam radius the axial size of the plasma decreases, the maximum temperature diminishes from 10 to 6 eV, Fig 15a. In all the cases the temperature maximum is located at a distance of beam radius from the surface $z \approx r_f$. This fact co-incides with the density distributions in Fig. 15b: just at this distance marked by vertical dashes the intensive drop of the density begins and just here proceeds the most intensive laser energy release and heating of the plasma.



a)



b)

Fig. 8. Contour plots of plasma electron concentration: a) and ionization degree: b) at $t = 120\text{ns}$

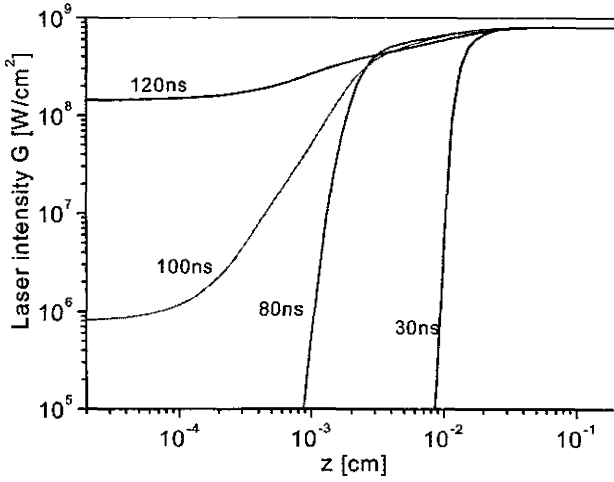


Fig. 9. Incident laser intensity profiles at the beam axis

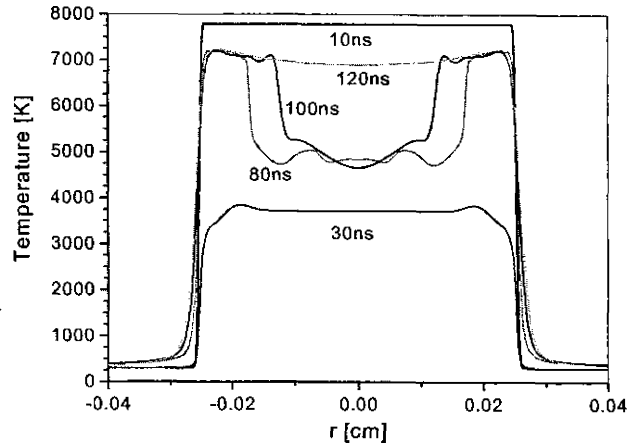


Fig. 10. Surface temperature profiles vs radius

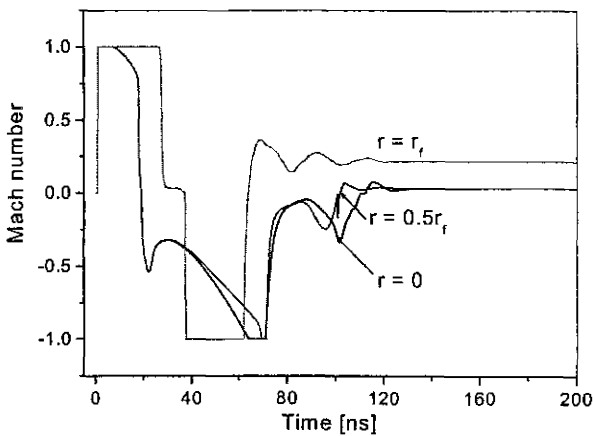


Fig. 11. Mach number vs time at different radial points

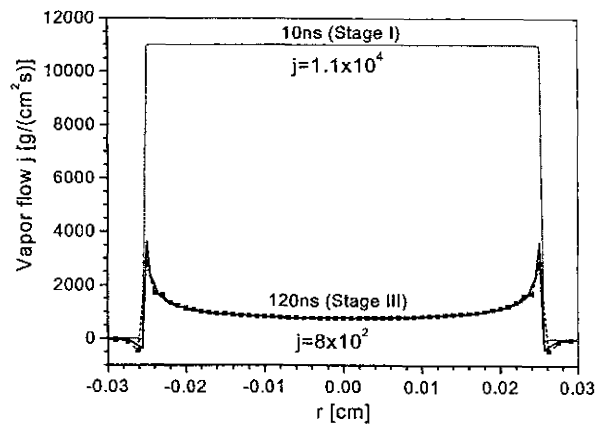


Fig. 12. Vapor flow (mass loss rate) profiles vs radius at the target surface

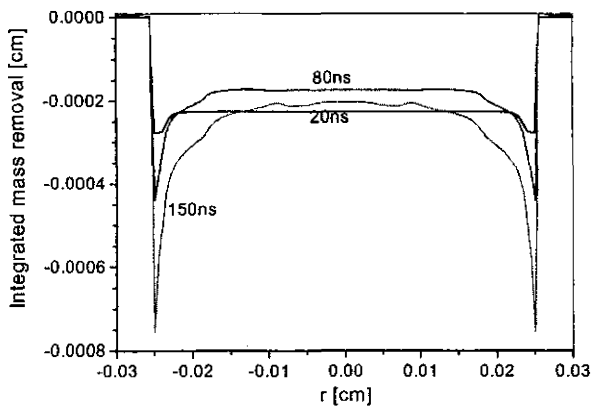


Fig. 13. Integrated mass removal vs radius

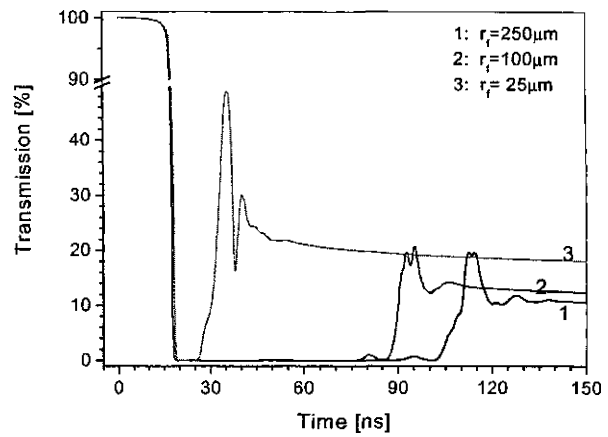


Fig. 14. Transmission coefficients for the action with different beam radius $r_f=250, 100, 25\mu\text{m}$

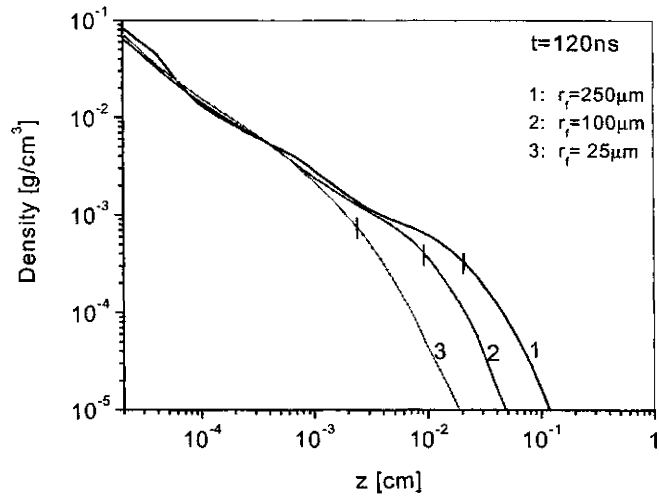
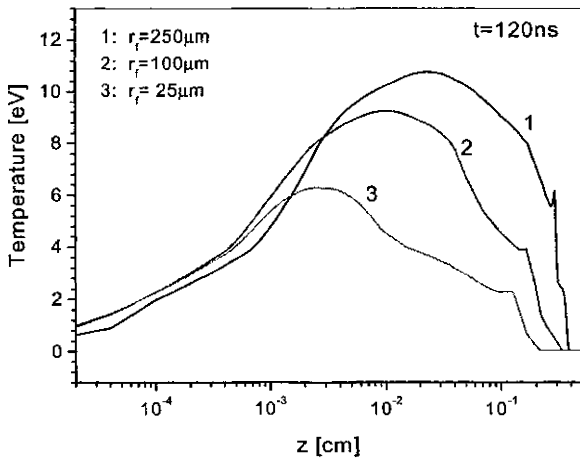


Fig. 15. Plasma temperature: a) and density: b) profiles at the beam axis for different beam radius $r_f=250, 100, 25\mu\text{m}$

Surface temperature and Mach number versus radius plots at $t=120\text{ns}$ predicted for the action with three different beam radius are depicted in Fig. 16. The smaller is the radius the high temperature is reached on the surface due to more transparent plasma and more intensive laser heating, Fig. 16a. In all the cases the temperature increases slowly from the center toward the beam edges. For the two larger beam radii $r_f = 250\mu\text{m}$ and $r_f = 100\mu\text{m}$ the radial dependencies of Mach number, Fig. 16b, have near the same shape and amplitude – constant value of ≈ 0.03 in the center part and sharp increase in narrow zone $\Delta r \approx 25\mu\text{m}$ near the beam boundary, where the evaporation proceeds easier due to lateral expansion and lower counter-pressure. For the smallest radius $r_f = 25\mu\text{m}$ the lateral expansion influence reaches the beam center therefore the evaporation here proceeds with higher Mach number $M \approx 0.05$

The amount of material removed versus radius plots for the three action regimes are shown in Fig. 17, $t = 120\text{ns}$. The action with smaller radius allows to evaporate more material. The difference is the most pronounced in the beam center where the predicted crater depth for the smallest radius reaches $4\mu\text{m}$, while for the larger beams this value is smaller by a factor of two.

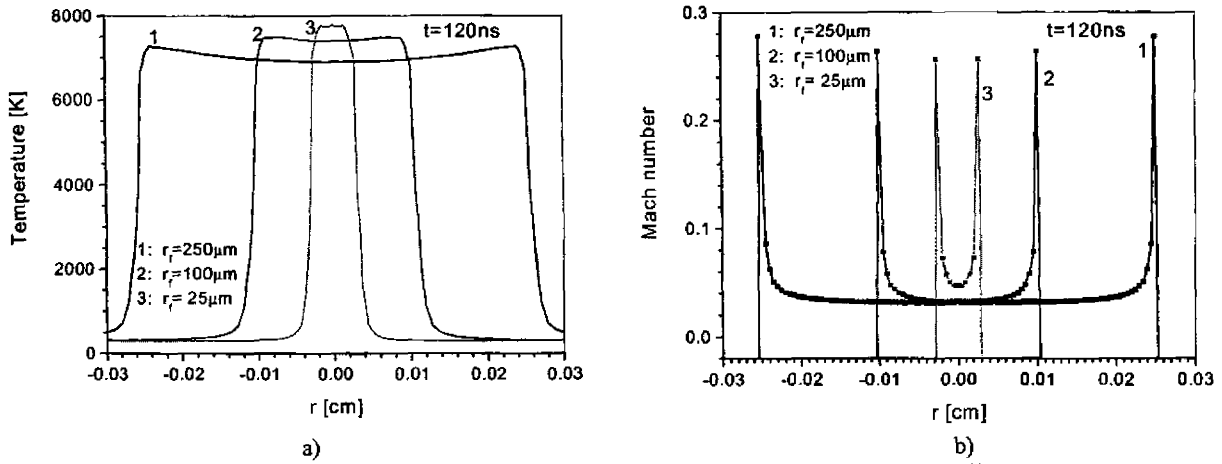


Fig. 16. Plasma surface temperature: a) and Mach number: b) profiles versus r for different beam radius

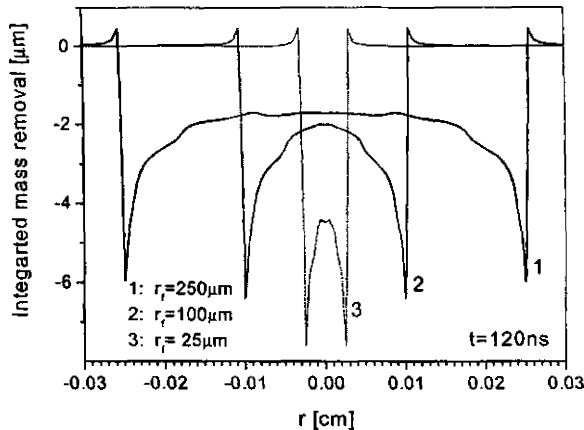


Fig. 17. Integrated mass removal vs r for different beam radius

4. CONCLUSION

The performed studies allow to draw the following conclusions on phase transition of Al surface induced by laser irradiation in vacuum with the intensity of $8 \times 10^8 \text{ W/cm}^2$ and the wavelength of $1.06 \mu\text{m}$:

- Phase transition of the target surface is controlled by the two factors: the surface temperature that depends on transmitted radiation intensity and the plasma pressure, governed by the expansion regime. The process comes through three characteristics stages – the sonic evaporation at the beginning, the condensation during the period of plasma formation and initial expansion and, finally, the recommence of evaporation in subsonic regime after the partial brightening of the plasma.
- During the subsonic evaporation stage the vapour flow and the mass removal rate is much higher near the beam boundaries than in the centre due to smaller plasma counter-pressure.
- The vapour plasma pattern is characterised by the dense hot zone near the surface at the distance of an order of the beam radius where the deposition of laser energy occurs, and rapid decrease of density outside the zone due to three-dimensional expansion.
- The application of the laser beam of smaller radius at the same intensity leads to the formation of more rarefied and more transparent plasma, that allows to improve the mass removal efficiency.

5. REFERENCES

1. W.W. Duley, "UV Lasers: effects and applications in material science", Cambridge University Press, Cambridge, 1996.
2. C. Phipps, R. Dreyfus, "Laser ablation and plasma formation", In: *Laser Microprobe Mass Analysis*, edited by A. Vertcs, R. Gijbels, F. Adams, pp. 2 – 57, John Wiley & Sons, New-York, 1993.
3. A. A. Samokhin, "Effect of laser radiation on absorbing condensed matter" Ed. A. V. Prokhorov, *Proc. of General Physics Institute USSR Academy of Science* 13, Nova Science, New York, 1990.

4. Ch. J. Knight, "Theoretical modeling of Rapid Surface Vaporization with Back Pressure", *ALAA Journal* 17, pp. 519 – 523, 1979.
5. S. I. Anisimov, "Vaporization of metal absorbing laser radiation", *Sov. Phys. JETP* 27, pp. 339 – 342, 1968
6. V. I. Mazhukin, A.A. Samokhin, "Phase transition kinetics under laser evaporation", *Sov. J. Quant. Elec.* 12, pp. 2432 – 2437, 1985.
7. V. I. Mazhukin, A. A. Samarskii, "Mathematical Modeling in the Technology of Laser Treatments of Materials", *Surveys on Mathematics for Industry* 4, pp. 85 – 149, 1994.
8. M. Aden, E. Beyer, R. Herziger, H. Kunze, "Laser – induced vaporization of a metal surface", *J. Phys. D: Appl. Phys.* 25, pp. 57 – 65, 1992.
9. P. V. Breslavskii, V. I. Mazhukin, "Mathematical modeling of laser – induced surface evaporation into medium with counter – pressure", Preprint of Institute of Mathematical Modeling Russian Academy of Science #2, 1992.
10. R. Kelly, A. Miotello, "Laser – pulse sputtering of atoms and molecules", *Nucl. Instr. Meth.* B91, pp. 682 – 690, 1994.
11. J. R. Ho, C. P. Grogopoulos, J. A. Humphrey, "Computational study of heat transfer and gas dynamics in the pulsed laser evaporation of metals", *J. Appl. Phys.* 78, 4696 – 4709, 1995.
12. A. V. Gusarov, A. G. Gnedovets, I. Smurov, "Gas dynamics of laser ablation : Influence of ambient atmosphere", *J. Appl. Phys.* 88, pp. 4352 – 4364, 2000.
13. V. Bergelson, I. Nemchinov, "Parameters of a plasma formed by the action of microsecond laser pulses an aluminum target in vacuum", *Sov. J. Quant. Elec.* 8, pp. 1198 – 1202, 1978.
14. V. I. Zubov, V. M. Krivcov, I. N. Naumova, Yu. D. Shmiglevskii, "Computation of laser radiation interaction with Al target and it's vapor", *J. Math. Phys. and Comp. Math* 20, pp. 1513 – 1524, 1980.
15. Yu. A. Stankevich, G. S. Romanov, "Computation of recoil pressure induced by optical radiation effect on absorbing surface in air", *Phys. and Chem. of Surf. Treat.* 4, pp. 15 – 23, 1981.
16. V. I. Mazhukin, G. A. Pestryakova, "Mathematical modeling of laser-induced surface evaporation", *DAN USSR* 278, pp. 843 – 847, 1984.
17. V. I. Mazhukin, G. A. Pestryakova, "Numerical algorithm for surface laser evaporation problem", *J. Comp. Math and Math Phys.* 25, pp. 1697 – 1709, 1985.
18. M. Aden, E. W. Kreutz, A.Voss, "Laser – induced plasma formation during pulsed laser deposition", *J. Phys. D: Appl. Phys.* 26, pp. 1545 – 1553, 1993.
19. A. Vertes, R. W. Dreyfus, D. E. Plat, "Modeling the thermal-to-plasma transitions for Cu photoablation", *IBM J. Res. Dev* 38, pp. 1 – 10, 1994.
20. G. Weyl, "Two-slab model of plasma mediated laser coupling to surfaces", *J. Thermophysics and Heat transfer* 8, pp. 229 – 235, 1994.
21. J. R. Ho, C. P. Grogopoulos, J. A. C. Humphrey, "Gas dynamics and radiation heat transfer in the vapor plume produced by pulsed laser irradiation of Al", *J. Appl. Phys.* 79, pp. 7205 – 7215, 1996.
22. H. S. Carslaw, J. G. Jaeger, "Conduction of heat in solids", Clarendon, Oxford, 1959.
23. B. N. Chetveruskin, "Dynamics of Radiative Gas", Nauka, Moskva, 1992.
24. V. I. Mazhukin, V. V. Nossov, I. Smurov, "Modeling of plasma dynamics at the air-water interface: Application to laser shock processing", *J. Appl. Phys.* 90, pp. 607 – 618, 2001.
25. Ya. B. Zeldovich, Yu. P. Raizer, "Physics of Shock waves and High Temperature Hydrodynamics Phenomena I", Academic, New York, 1967.
26. G. S. Romanov, Yu. A. Stankevich, L. K. Stankevich, K. L. Stepanov, "Thermodynamic and optical properties of gases in a wide range of parameters", *Int. J. Heat Mass Transfer* 38, pp. 545 – 556, 1995.
27. D. Crout, "An application of kinetic theory to the problems of evaporation and sublimation of monatomic gases", *J. Math. Phys.* 15, pp. 1 – 54, 1936.
28. V. I. Mazhukin, P. A. Prudkovskii, A. A. Samokhin, "About gas – dynamical boundary conditions on evaporation front", *J. Mathematical Modeling* 6, pp. 3 – 10, 1993.
29. Y. Sone, S. Takata, F. Golse, "Notes on the boundary conditions for fluid-dynamic equations on the interface of a gas and its condensed phase", *Phys. Fluids* 13, pp. 324 – 334, 2001.
30. A. P. Kryukov, "Kinetic Analysis of the Processes of Evaporation and Condensation on a Surface", *Heat Transfer Research* 24, pp. 984 – 998, 1992.
31. K. Aoki, Y. Sone, T. Yamada, " Numerical analysis of gas flows condensing on its plane condensed phase on the basis of kinetic theory", *Phys. Fluids A* 2, pp. 1867 – 1878, 1990.
32. A. V. Gusarov, I. Smurov, "Gas – dynamic boundary conditions of evaporation and condensation : Numerical analysis of the Knudsen layer", *Phys. Fluids* 14, pp. 4242 – 4255, 2002.
33. A.A. Samarskii, "Theory of finite – difference scheme", Science, Moscow, 1977.
34. V. I. Mazhukin, I. Smurov, G. Flamant, "Simulation of Laser Plasma Dynamics: Influence of Ambient Pressure and Intensity of Laser Radiation", *J. Comp. Phys.* 112, pp. 78 – 90, 1994.